Electronic Supplementary Material (ESI) for Physical Chemistry Chemical Physics
This journal is © The Owner Societies 2012

Supplementary Information for "Non Hexagonal Ice at Hexagonal Surfaces: The Role of Lattice Mismatch"

Stephen J. Cox,[1] Shawn M. Kathmann,[2] John A. Purton,[3] Michael J. Gillan,[4] and Angelos Michaelides[1]

[1)] *Thomas Young Centre, London Centre for Nanotechnology and Department of Chemistry, University College London, London WC1E 6BT, United Kingdom*

[2)] *Chemical and Materials Sciences Division, Pacific Northwest National Laboratory, Richland, Washington 99352, United States*

[3)] *STFC, Daresbury Laboratory, Warrington WA4 4AD, U.K.*

[4)] *Thomas Young Centre, London Centre for Nanotechnology and Department of Physics and Astronomy, University College London, London WC1E 6BT, U.K.*

(Dated: 27 February 2012)

I. SUMMARY

This supplementary information includes details of the two model surfaces used, along with additional results not presented in the main text, including those using the SPC/E water model. A brief comparison of cluster energies using TIP4P to Møller-Plesset perturbation theory is also included.

II. HONEYCOMB SURFACE

The surface was represented by a hexagonal close packed array of points, separated by a lattice constant $a_{0,S}$, consisting of four layers (see Fig. S1). The parameters used in this LJ potential are $\sigma_{OS} = 3.34596$ Å and $\epsilon_{OS} = 6.990697$ kJ/mol and were chosen to give monomer adsorption energies that were comparable to the TIP4P dimer binding energy (-26.09 kJ/mol)[1]. Keeping the LJ parameters fixed for different lattice spacings did lead to only a slight change in monomer adsorption energies (see Table S1). To test whether or not this change in binding energy significantly affects the results, we apply a 'trial-and-error' approach to varying the Lennard-Jones well depth until the monomer binding energy of the $\delta = 0.07$ surface is approximately that of the $\delta = 0.00$ surface. We then performed a GCMC simulation on this modified $\delta = 0.07$ surface at $\mu = -49.8$ kJ/mol and analysed the resulting structure, averaging over a 15 K canonical MC simulation. The radial distribution functions of the original and modified surfaces are given in Fig. S2, where it can be seen that the structures are, to all intents and purposes, identical. This gives us reason to believe that any change in structures seen at the other surfaces is due to the change in lattice constant and not due to any change in binding energy to the surface.

III. HCP SURFACE

The external potential $V_{\text{ext}}(x_{\text{ox}}, y_{\text{ox}}, z_{\text{ox}})$ described qualitatively in the main text can be defined more formally as:

$$V_{\text{ext}}(x_{\text{ox}}, y_{\text{ox}}, z_{\text{ox}}) = F(x_{\text{ox}}, y_{\text{ox}}) V_{\text{Morse}}(z_{\text{ox}}) \tag{1}$$

where $x_{\text{ox}}, y_{\text{ox}}, z_{\text{ox}}$ are the coordinates of the water oxygen atom, $V_{\text{Morse}}(z_{\text{ox}})$ is a Morse

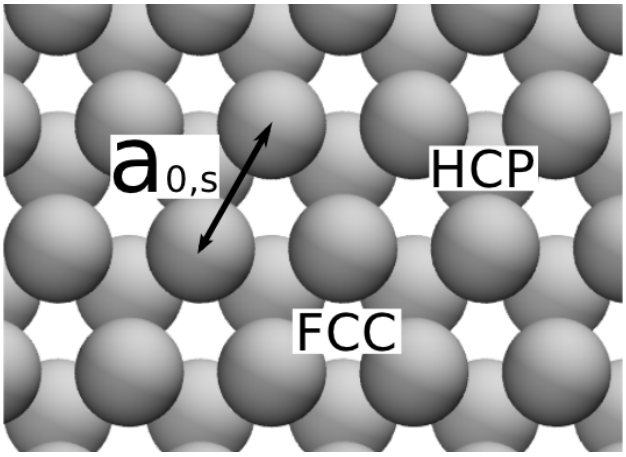

FIG. S1. **Schematic of the model honeycomb surface**. The surface lattice constant ($a_{0,S}$) is the nearest neighbour distance between coplanar sites. The potential minima for monomer adsorption are found at the HCP and FCC sites labelled in the diagram.

δ	$a_{0,S}$ (Å)	E_{bind} (kJ/mol)
−0.14	3.818	-32.93 ± 0.05
−0.07	4.307	-30.42 ± 0.05
0.00	4.440	-28.64 ± 0.05
0.04	4.618	-28.44 ± 0.07
0.07	4.751	-27.36 ± 0.05

TABLE S1. **Binding Energies for a water monomer on the different honeycomb surfaces.**

potential dependent only on the normal distance of the water molecule from the surface and $F(x_{\rm ox}, y_{\rm ox})$ is a modulating function, dependent on the lateral displacement of the water molecule. The explicit forms of these functions are:

$$V_{\rm Morse}(z_{\rm ox}) = D_{z0}\{1 - \exp\left[-k_z(z_{\rm ox} - z_0)\right]\}^2 - D_{z0} \tag{2}$$

$$F(x_{\rm ox}\,,\, y_{\rm ox}) = \delta E_{frac}\left[\left(\frac{1-\delta E_{frac}}{\delta E_{frac}} - f(x_{\rm ox}\,,\, y_{\rm ox})\right)\right] \tag{3}$$

and

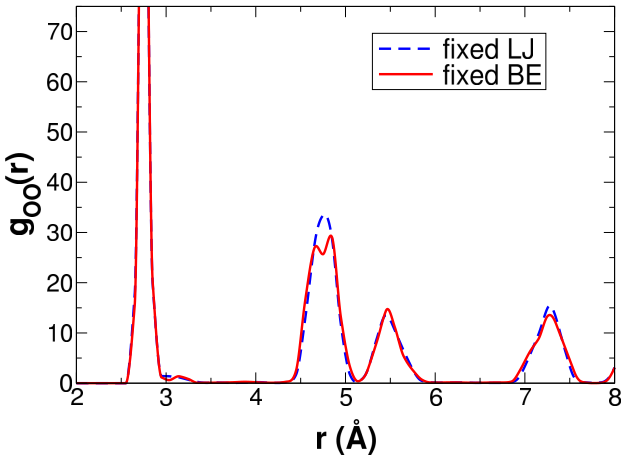

FIG. S2. **Radial distribution function comparison** of the $\delta = 0.07$ surface with fixed Lennard-Jones parameters (dashed blue line) and with the Lennard-Jones parameters increased (solid red line) to give a binding energy approximately that of the $\delta = 0.00$ surface (28.65 and 28.64 kJ/mol respectively).

$$\begin{aligned} f(x_{\text{ox}}\,,\,y_{\text{ox}}) = &\left(1-\exp\left[-k_{xy}\left(x_{\text{ox}}^2+y_{\text{ox}}^2\right)^{\frac{1}{2}}\right]\right)^2-1 \\ &+\left(1-\exp\left[-k_{xy}\left((x_{\text{ox}}-x_1)^2+(y_{\text{ox}}-y_1)^2\right)^{\frac{1}{2}}\right]\right)^2-1 \\ &+\left(1-\exp\left[-k_{xy}\left((x_{\text{ox}}-x_1)^2+(y_{\text{ox}}+y_1)^2\right)^{\frac{1}{2}}\right]\right)^2-1 \\ &+\left(1-\exp\left[-k_{xy}\left((x_{\text{ox}}+x_1)^2+(y_{\text{ox}}-y_1)^2\right)^{\frac{1}{2}}\right]\right)^2-1 \\ &+\left(1-\exp\left[-k_{xy}\left((x_{\text{ox}}+x_1)^2+(y_{\text{ox}}+y_1)^2\right)^{\frac{1}{2}}\right]\right)^2-1 \end{aligned} \tag{4}$$

where D_{z0} is the well-depth of the potential perpendicular to the surface, k_z controls the width of the potential and z_0 is the position of the potential energy minimum above the surface. The function $f(x_{\text{ox}}\,,\,y_{\text{ox}})$ is composed of five symmetrised Morse potentials of unit depth, whose width is determined by k_{xy}, centred at $(0,0)$, (x_1,y_1), $(x_1,-y_1)$, $(-x_1,y_1)$ and $(-x_1,-y_1)$ where $x_1 = a_{0,S}/2\sqrt{3}$ and $y_1 = a_{0,S}/2$. As written above, $f(x_{\text{ox}}\,,\,y_{\text{ox}})$ is defined for the interval $-x_1 \leq x_{\text{ox}} < x_1\,,\,-y_1 \leq y_{\text{ox}} < y_1$ and is periodic such that:

$$f(x_{\text{ox}}+2x_1\,,\,y_{\text{ox}}+2y_1) = f(x_{\text{ox}}\,,\,y_{\text{ox}}) \tag{5}$$

The parameter δE_{frac} controls the barrier height and is defined as the fractional difference

between the energy at one of the minima E_{min} and the energy at the top of the barrier between minima $E^{\ddagger}$:

$$\delta E_{frac} = \frac{E^{\ddagger} - E_{min}}{|E_{min}|} \tag{6}$$

By choosing the width of the Morse potential sites in $f(x_{\text{ox}}\,,\,y_{\text{ox}})$ so that neighbouring sites only minimally interact, we can exert almost complete control over the barrier height. A schematic of the this surface potential is shown in Fig. S3.

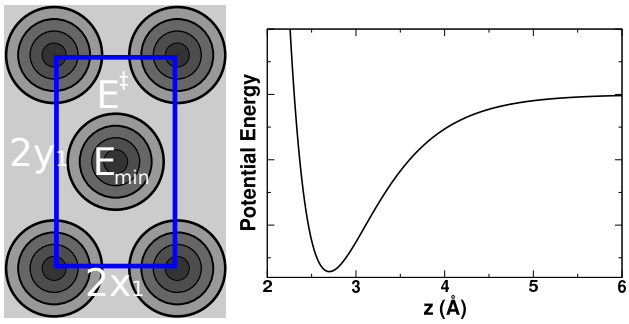

FIG. S3. **Schematic of the external potential**. The modulating function, $f(x_{\text{ox}}\,,\,y_{\text{ox}})$ is shown on the left and the Morse potential perpendicular to the surface is shown on the right. When $(x_{\text{ox}}\,,\,y_{\text{ox}})$ are at the centre of one of the symmetrised Morse functions shown on the left, the potential acting along z is left unchanged. For regions in between the symmetrised Morse functions, the z-component of the potential is increased up to a maximum value $E^{\ddagger}$, as determined by the parameter δE_{frac}.

The parameters used to define the external potential are given in Table S2. The value for D_{z0} and δE_{frac} were taken from DFT calculations for a water monomer on Ag(111) that account accurately for the role of dispersion[2]. The width of the symmetrised Morse functions varied between surfaces such that the product of k_{xy} and the nearest neighbour distance remained constant, ensuring that the barrier height between minima on the different surfaces stayed the same.

IV. ASSESSMENT OF THE WATER-SURFACE INTERACTION

Obviously, both these surfaces are somewhat simplified when one considers the potentials exerted on water molecules by real surfaces and if we were attempting to accurately deter-

mine surface structures, sophisticated, system dependent, water–surface potentials would be required. Perhaps the most drastic simplification in our systems is that only the oxygen atoms are coupled to the surface and that the hydrogen atoms can vary their positions independently of the surface. We justify this simplification by noting that the traditional theory, to which we wish to compare, only makes reference to the relative positions of adsorption sites and does not account for any orientational dependence of the water molecules at the surface. In order to check that the lack of orientational dependence is not biasing the formation of non-bilayer overlayers, we have performed a GCMC simulation on the $\delta = 0.00$ HCP surface with a Morse potential acting on the z-component of the hydrogen atoms. A snapshot from this simulation is shown in Fig. S4, where it can be seen that including this hydrogen term does not promote the formation of an ice-like bilayer. This hydrogen term was chosen arbitrarily, and the values are shown in Table S3 (in general, it is not possible to decouple the hydrogen and oxygen interactions with the surface). However, by doing this, we demonstrate that concerns regarding the hydrogen atoms approaching too close to the surface favouring non-bilayer structures is not the case with these simple potentials.

Parameter	Value
D_{z0}	27.112 kJ/mol
k_z	1.75 Å^{-1}
z_0	2.7 Å
δE_{frac}	0.30605
$k_{xy} \times \frac{a_{0,S}}{\sqrt{3}}$	18.0

TABLE S2. **Parameters used to define the external potential.**

Furthermore, we can examine the results of previously reported DFT calculations on bilayers at Cu(110) and Ru(0001) (see the Ref. 3 and its supporting information) in order to assess how important the hydrogen interaction with the surface is in influencing the oxygen corrugation and overall hydrogen bonding. The results from this DFT study (using the optB88-vdW density functional) are presented in Table S4.

Let us begin by comparing the H-down and H-up bilayers on Cu(110). For the H-down bilayer, we can see that there is very little difference in binding heights of the water oxygens

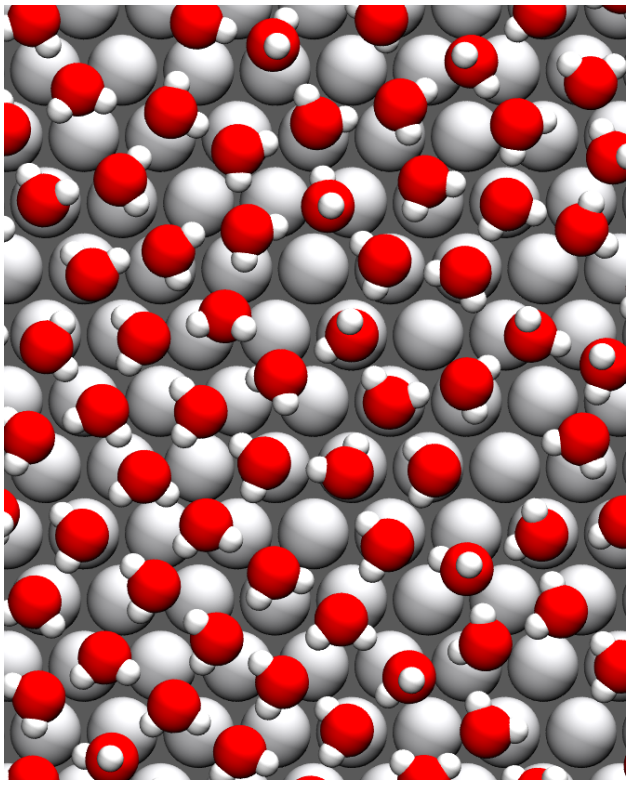

FIG. S4. **Snapshot of a GCMC simulation on the HCP $\delta = 0.00$ surface with a Morse potential acting on the hydrogen atoms.** We can see that inclusion of a potential of the hydrogen atoms (preventing close approach to the surface) does not promote ice-like bilayer formation.

($\Delta z_{\mathrm{O}} = 0.055\,\mathrm{\AA}$) between the flat lying water molecules and those water molecules with one of their hydrogens pointed towards the surface, whereas in the case of the H-up bilayer, there is a far greater difference in binding heights ($\Delta z_{\mathrm{O}} = 0.776\,\mathrm{\AA}$). This increase in the buckling of the H-up bilayer is accompanied by an increase in the water-water bonding ($E_{\mathrm{gas}}^{\mathrm{H_2O-H_2O}} = -440$ meV/$\mathrm{H_2O}$) relative to the H-down bilayer ($E_{\mathrm{gas}}^{\mathrm{H_2O-H_2O}} = -422$ meV/$\mathrm{H_2O}$). However, the H-down bilayer, with its lower Δz_{O}, is overall more stable than the H-up bilayer and this is due to an increased binding with the surface ($E_{\mathrm{ads}}^{\mathrm{H_2O-Cu}} = -259$ and -178 meV/$\mathrm{H_2O}$ respectively). The findings that a buckling gives better water bonding, but that relaxation along the surface normal can outweigh this effect, are consistent with the conclusions in the main text (see Fig. 4). If we look at the bilayers on Ru(0001), we again see a similar trend, although the H-down and H-up bilayers have essentially identical adsorption energies.

In general, optimised H-down bilayers on metal surfaces tend to be flat relative to bulk ice

Parameter	Value
D_{z0}, Oxygen	17.112 kJ/mol
D_{z0}, Hydrogen	5.000 kJ/mol
k_z, Oxygen	1.75 Å^{-1}
k_z, Hydrogen	1.75 Å^{-1}
z_0, Oxygen	2.7 Å
z_0, Hydrogen	2.72 Å
δE_{frac}, Oxygen	0.30605
$k_{xy} \times \frac{a_{0,S}}{\sqrt{3}}$, Oxygen	18.0

TABLE S3. **Parameters used to define the external potential with hydrogen parameters.** The choices for the hydrogen parameters we chosen such that the total monomer binding energy was unchanged from the simulation set-up described in Table S2. The potential on the hydrogen atoms only acts on the z-component of their positions.

(see e.g. Refs. 4 and 5), as is also the case on the hydroxylated kaolinite (001) surface[6]. This suggests that by only including the oxygen interaction with the surface, we are not ignoring an interaction that will structure the first layer into a highly corrugated bilayer. In fact, decomposition of DFT energies shows that stabilisation of corrugated water overlayers arises from augmentation of the hydrogen bonding interaction between water molecules, consistent with our findings, and not due to a repulsive interaction of the hydrogen with the surface.

V. WATER BINDING HEIGHT ABOVE SURFACE

As mentioned in the main text, the water molecules all bind at near equal heights above the surface. Fig. S5 shows a histogram of water oxygen heights above the HCP surface and snapshot from the honeycomb surface to demonstrate this fact.

		H-down	H-up
Cu(110)	E_{ads}	-681	-618
	$E_{\mathrm{gas}}^{\mathrm{H_2O-H_2O}}$	-422	-440
	$E_{\mathrm{ads}}^{\mathrm{H_2O-Cu}}$	-259	-178
	Δz_{O} (Å)	0.055	0.776
Ru(0001)	E_{ads}	-667	-666
	$E_{\mathrm{gas}}^{\mathrm{H_2O-H_2O}}$	-382	-447
	$E_{\mathrm{ads}}^{\mathrm{H_2O-Ru}}$	-285	-219
	Δz_{O} (Å)	0.516	0.771

TABLE S4. **Adsorption energies (E_{ads}) of different water overlayers and their decompositions on Cu(110) and Ru(0001).** $E_{\mathrm{gas}}^{\mathrm{H_2O-H_2O}}$ is the energy of the fixed water layer (optimised at the surface) in the gas phase, $E_{\mathrm{ads}}^{\mathrm{H_2O-M}}$ is the binding energy due to water–metal interactions and Δz_{O} is the difference in heights of the water molecules above the surface.

VI. RESULTS FROM HONEYCOMB SURFACE

Figure S6 shows the RDFs on the honeycomb surfaces. As we can see, the results are qualitatively similar to those on the HCP surfaces. We can compare the energetics of the different overlayers by varying the depth of the Lennard-Jones potential on each surface until the binding energy roughly matches that of the $\delta = 0.00$ surface and performing a new set of canonical MC simulations without the need for a new set of GCMC simulations. The binding energies for the new surfaces are given in Table S5. From Fig. S7 we can see that the contribution to the total energy from the water–water interactions remains effectively constant on all surfaces, that is, there is no significant energy cost in forming disordered structures on the compressed surfaces. We can also see that the total energy is reasonably flat with the disregistry, with a slight stabilisation going from $\delta = 0.04$ to $\delta = 0.07$. As the water-water interactions are similar across-the-board, we conclude that this stabilisation arises from increased binding to the surface. This result is not surprising given the similarity between $r_{0,i}$ (2.75 Å) and $r_{0,S}$ on the $\delta = 0.07$ surface (2.74 Å).

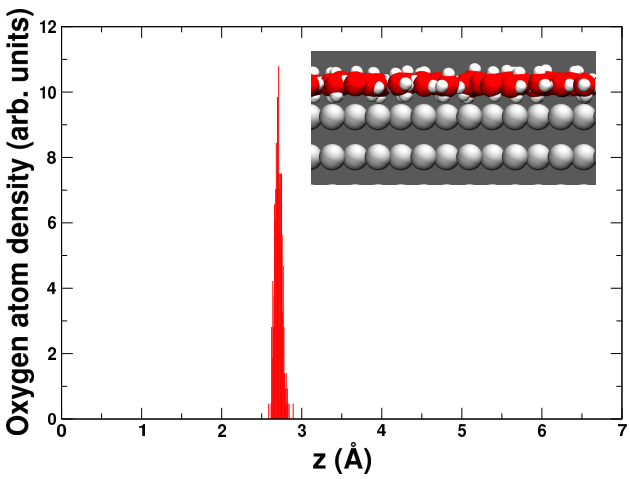

FIG. S5. **Histogram of water oxygen heights above one of the HCP surfaces.** All water molecules are bound within 0.5 Å of each other. The inset shows a snapshot from one of the honeycomb surfaces, showing that the water molecules bind at near equal heights. The data shown is representative of all surfaces and therefore for clarity, we do not show data from the other surfaces.

δ	ϵ (kJ/mol)	E_{bind} (kJ/mol)
-0.14	6.081	-28.64
-0.07	6.584	-28.65
0.00	6.991	-28.64
0.04	7.036	-28.62
0.07	7.321	-28.65

TABLE S5. **Altered Lennard-Jones depths and new binding energies**. The $\delta = 0.00$ remained unchanged. The width of the LJ potential potential ($\sigma = 3.346$ Å) was left unchanged.

VII. RESULTS USING SPC/E WATER

To test how dependent our results are on the choice of water model, we performed the same set of simulations using SPC/E water. Before presenting the results, it should be noted that the SPC/E water dimer is even more tightly binding than the TIP4P dimer (the dimer binding energy of SPC/E is -30.1 kJ/mol).[7] This means that although the water–

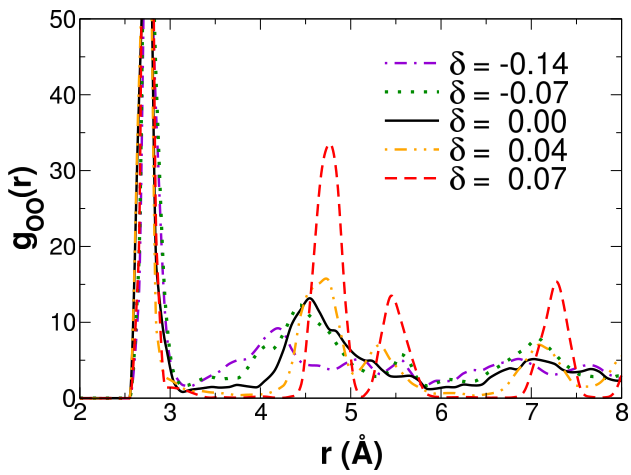

FIG. S6. **Radial distribution functions for different δ (honeycomb surface).** As on the HCP surfaces, the position of the nearest–neighbour peak is essentially invariant as the substrate lattice constant is changed, located at approximately 2.75 Å.

water and water–surface interactions are still comparable, the water–water interactions are slightly stronger, in contrast to the TIP4P simulations. The GCMC simulations on the honeycomb surfaces were performed using the parameters that gave near equal binding on all surfaces (see Table S5). Fig. S7 and S9 shows the energy profiles using SPC/E water. The agreement between the two water models is good, with some small differences on the honeycomb surfaces with compressed δ, probably owing to the differences in water–water binding.

VIII. COMPARISON TO MØLLER-PLESSET THEORY

Due to the non-ice-like structures found on the HCP surface, we decided to compare the binding energies of various six water molecule clusters in the gas phase using MP2 and TIP4P. The clusters were taken from surfaces with different values of δ and were chosen to give a range of bonding motifs. The results are presented in Fig. S10 where it is clear that TIP4P overbinds the six molecule clusters. Taking the difference between the TIP4P and MP2 binding energies we can see that this overbinding is not constant for the clusters studied. However there is no obvious bias for any particular type of structure and we therefore feel confident that the structures seen are not an artifact of the water potential used.

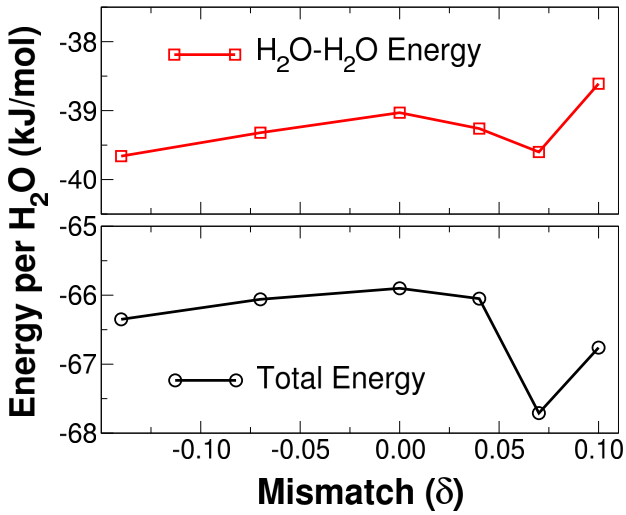

FIG. S7. **Energies of the different overlayers on the honeycomb surface.** The water–water energy was calculated by removing the surface from the final configuration from the canonical MC runs and performing single point energy calculations on the remaining water structures. The figure shows that there is very little change in water–water interaction for the different surfaces. The total energy was calculated from averages over the canonical MC runs. Again, there is little change in energy from changing $a_{0,S}$ except on the $\delta = 0.07$ surface where there is a slight stabilisation. As the water–water energy remains almost constant, we conclude that this is due to an increase in the water–surface interaction.

MP2 calculations were performed using the GAUSSIAN 09[8] package using the AUG-cc-pVDZ basis set[9]. The binding energies using TIP4P were performed using DL_MONTE, in $100 \times 100 \times 100$ Å^3 box using a full Ewald summation.

REFERENCES

[1]D. J. Wales and M. P. Hodges, Chem. Phys. Lett. **286**, 65 (1998).

[2]J. Carrasco, J. Klimeš, and A. Michaelides, (unpublished).

[3]J. Carrasco, B. Santra, J. Klimes, and A. Michaelides, Phys. Rev. Lett. **106** (2011).

[4]A. Michaelides, A. Alavi, and D. A. King, Phys. Rev. B **69**, 113404 (2004).

[5]S. Meng, E. G. Wang, and S. Gao, Phys. Rev. B **69**, 195404 (2004).

[6]X. L. Hu and A. Michaelides, Surf. Sci. **602**, 960 (2008).

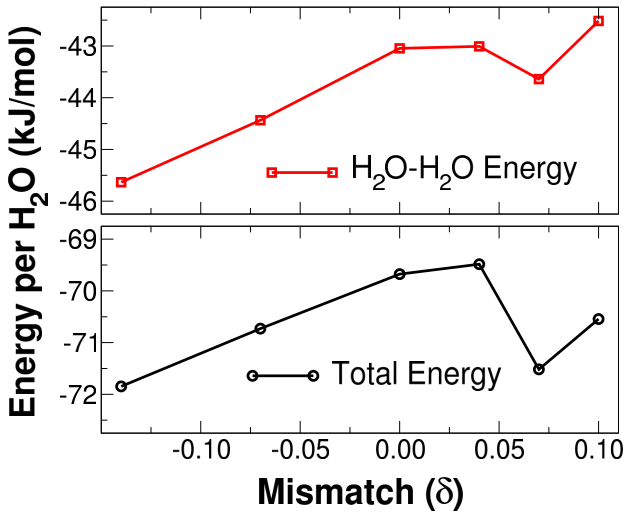

FIG. S8. **Energies of the different overlayers on the honeycomb surfaces using SPC/E water.** On the whole we see a similar trend to TIP4P, except that the total energy at compressed δ is relatively more stable. As we can see, this arises from an increase in the water–water interaction, which may be expected due to tighter binding of SPC/E water.

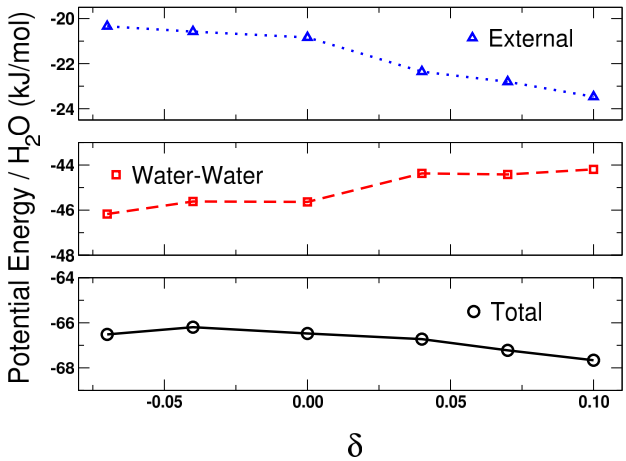

FIG. S9. **Energies of the different overlayers on the HCP surface using SPC/E water.** The agreement with the TIP4P simulations is very good (c.f. Fig. 3, main text).

[7]B. Chen, J. Xing, and J. Siepmann, J. Phys. Chem. B **104**, 2391 (2000).

[8]M. J. Frisch, G. W. Trucks, H. B. Schlegel, G. E. Scuseria, M. A. Robb, J. R. Cheeseman, G. Scalmani, V. Barone, B. Mennucci, G. A. Petersson, H. Nakatsuji, M. Caricato, X. Li, H. P. Hratchian, A. F. Izmaylov, J. Bloino, G. Zheng, J. L. Sonnenberg, M. Hada, M. Ehara,

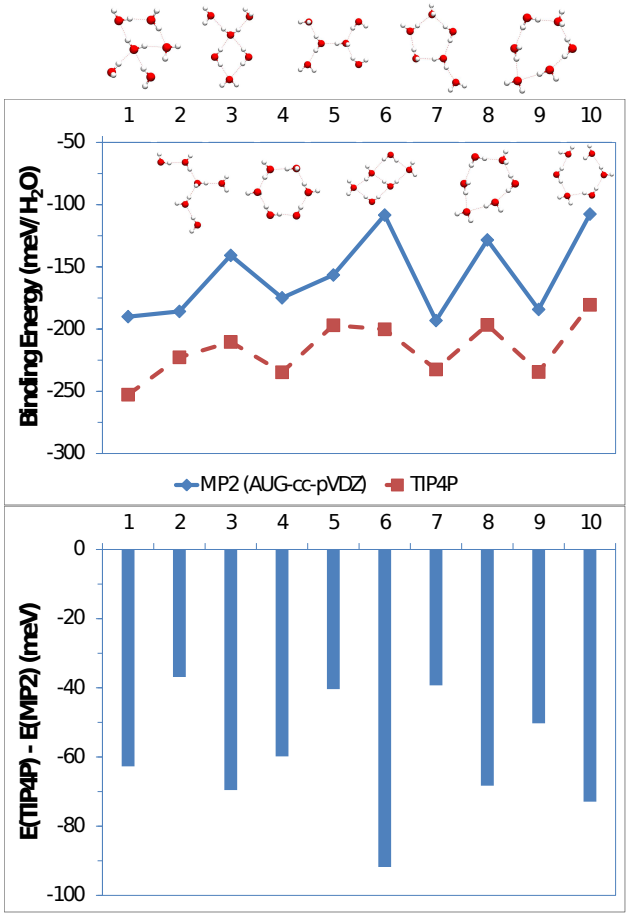

FIG. S10. **Binding energies of water hexamers from different overlayers using TIP4P and MP2.** The top panel shows the total binding energies for 10 clusters using both methods and the bottom panel shows the difference in binding energies using TIP4P and MP2 (E(TIP4P) $-$ E(MP2)). Clearly, TIP4P overbinds all of the clusters with varying degree. However, there is no obvious systematic bias towards ice-like or non-ice-like structures.

K. Toyota, R. Fukuda, J. Hasegawa, M. Ishida, T. Nakajima, Y. Honda, O. Kitao, H. Nakai, T. Vreven, J. A. Montgomery, Jr., J. E. Peralta, F. Ogliaro, M. Bearpark, J. J. Heyd, E. Brothers, K. N. Kudin, V. N. Staroverov, R. Kobayashi, J. Normand, K. Raghavachari, A. Rendell, J. C. Burant, S. S. Iyengar, J. Tomasi, M. Cossi, N. Rega, J. M. Millam, M. Klene, J. E. Knox, J. B. Cross, V. Bakken, C. Adamo, J. Jaramillo, R. Gomperts, R. E. Stratmann, O. Yazyev, A. J. Austin, R. Cammi, C. Pomelli, J. W. Ochterski, R. L. Martin, K. Morokuma, V. G. Zakrzewski, G. A. Voth, P. Salvador, J. J. Dannenberg, S. Dapprich, A. D. Daniels, Ã. Farkas, J. B. Foresman, J. V. Ortiz, J. Cioslowski, and D. J. Fox,

"Gaussian 09 Revision A.2,".

[9]T. H. Dunning, J. Chem. Phys. **90** (1989).